Reaction of O_2 with the Hydrogen Atom in Water up to 350 °C

Ireneusz Janik and David M. Bartels*

Notre Dame Radiation Laboratory, Notre Dame, Indiana 46556

Timothy W. Marin

Chemistry Department, Benedictine University, Lisle, Illinois 60532

Charles D. Jonah

Chemistry Division, Argonne National Laboratory, Argonne, Illinois 60439

Received: August 9, 2006; In Final Form: October 27, 2006

The reaction of the $H^\bullet$ atom with O_2, giving the hydroperoxyl $HO_2^\bullet$ radical, has been investigated in pressurized water up to 350 °C using pulse radiolysis and deep-UV transient absorption spectroscopy. The reaction rate behavior is highly non-Arrhenius, with near diffusion-limited behavior at room temperature, increasing to a near constant limiting value of $\sim 5 \times 10^{10}$ M^{-1} s^{-1} above 250 °C. The high-temperature rate constant is in near-perfect agreement with experimental extrapolations and ab initio calculations of the gas-phase high-pressure limiting rate. As part of the study, reaction of the $OH^\bullet$ radical with H_2 has been reevaluated at 350 °C, giving a rate constant of $(6.0 \pm 0.5) \times 10^8$ M^{-1} s^{-1}. The mechanism of the $H^\bullet$ atom reaction with the $HO_2^\bullet$ radical is also investigated and discussed.

I. Introduction

The reaction of the $H^\bullet$ atom with aqueous O_2, forming the hydroperoxyl radical,

$$H^\bullet + O_2 \rightarrow HO_2^\bullet \quad (1)$$

is of central importance in combustion chemistry and has been carefully studied both experimentally[1,2] and via quantum chemistry.[3] The reaction in very-high-temperature water is of importance for supercritical water oxidation processes.[4] In water-cooled nuclear reactor chemistry, the reaction is an important step in "hydrogen water chemistry", whereby a slight overpressure of H_2 is used to reduce the radiolytically produced O_2 and H_2O_2 back to water.[5] It is important to be able to predict the minimum H_2 concentration needed to accomplish this kinetic trick, because excess H_2 may result in undesirable hydriding corrosion.

In the gas-phase formation of $HO_2^\bullet$, there is no barrier to O−H bond formation for approach of the $H^\bullet$ atom at about 45 degrees with respect to the O−O axis.[3] In room-temperature water, the measured reaction rate is consistent with nearly diffusion-limited behavior[6−9] and a barrierless reaction. The question is whether this remains true at elevated temperature, and whether the gas-phase potential is strongly perturbed by the aqueous environment. If not, the gas-phase measurements can be simply transferred to the aqueous-phase simulation problem.

In the present investigation, the reaction of $H^\bullet$ atoms and O_2 in pressurized water has been studied at temperatures up to 350 °C using pulse radiolysis and transient deep-ultraviolet absorption spectroscopy. The reaction demonstrates strongly non-Arrhenius behavior above 100 °C, with the rate constant apparently decreasing above 325 °C. In the discussion below, we show that the behavior for this reaction is entirely consistent with the gas-phase high-pressure limit. The mechanism for reaction of $H^\bullet$ atom with $HO_2^\bullet$ radical is also discussed.

II. Experimental Section

Electron pulse radiolysis/transient absorption experiments were carried out using 4−20 ns pulses from the Argonne Chemistry Division's 20 MeV electron linac accelerator. The sample cell, flow system, and basic experimental setup and characteristics were described in previous publications.[10,11] However, for the current measurements some changes were applied. Analyzing light from a pulsed 150 W xenon lamp (Osram XBO-150W/S) was selected using an ISA-545 double-grating monochromator. With this monochromator, there was no detectable scattered light from the visible or near-UV to distort the deep-UV absorption measurements. The detector was a five-stage Hamamatsu photomultiplier wired to deliver linear photocurrent up to 2 mA. To minimize the scattering loss of deep-UV analyzing light encountered over a potentially long optical path, the detector system was placed roughly 50 cm from the sample cell and shielded from the linac radiation with lead bricks.

The sample was mixed from three separate syringe pumps (ISCO-260C) working in constant flow mode. The total flow rate was 4 mL/min. The first pump contained water saturated with N_2O at room temperature, giving an N_2O concentration of 0.024 molal (*m*). The N_2O (AGA gas, Ultrahigh Purity) was first bubbled through a sparging vessel filled with a highly basic solution of pyrogallol to remove any traces of oxygen.[12] The second pump contained water saturated with O_2 (AGA gas, Ultrahigh Purity) at room temperature, giving an O_2 concentration of 0.0013 *m*. The third pump contained water pressurized

* Author to whom correspondence should be addressed. E-mail: bartels@hertz.rad.nd.edu. Phone: (574) 631-5561. Fax: (574) 631-8068.

10.1021/jp065140v CCC: $37.00
Published on Web 12/14/2006

with H_2 (AGA gas, Ultrahigh Purity) at room temperature. Pressurized H_2 samples were prepared in our laboratory-built high-pressure gas−liquid saturator.[13] The pressure of hydrogen in the saturator was constant for given samples of water used to refill the syringe pump but decreased in the course of several days of experiment. Typically, the hydrogen pressure ranged from 82 to 149 bar, giving aqueous hydrogen concentrations of 0.100−0.055 *m*.[14] The hydrogen concentration in the sample mix was constant for a given experiment and was always equal to 50% of the corresponding hydrogen concentration in the pressurized water saturator. The oxygen concentration in the sample was changed by changing the flow ratio between pumps delivering N_2O- and O_2-saturated water and was in the range 2.5×10^{-5} to 2.0×10^{-4} *m*. Correspondingly, the N_2O concentration was varied between 1.2×10^{-2} and 5.0×10^{-3} *m*. The total pressure in the system was adjusted with a back pressure regulator to 250 ± 0.1 bar. Normal temperature stability was ±0.3 °C.

Pulse radiolysis of water creates predominantly hydrated electrons (e_{aq}^-) and $OH^\bullet$ radicals, which are quickly converted to hydrogen atoms via reactions 2 and 3.

$$e_{aq}^- + N_2O \rightarrow OH^\bullet + N_2 + OH^- \quad (2)$$

$$OH^\bullet + H_2 \rightarrow H^\bullet + H_2O \quad (3)$$

In the limit of high oxygen concentration, reaction 1 becomes pseudo-first-order, and thus the reaction 1 rate constant, k_1, can be established by monitoring the increase of hydroperoxyl radical absorbance at 230 nm.[15] At room temperature, the pK_a for the $HO_2^\bullet$ radical is 4.8, and virtually all of the radical population converts to the basic $O_2^{\bullet-}$ form via reaction 4, giving

$$HO_2^\bullet \leftrightarrow O_2^{\bullet-} + H^+ \quad (4,\text{-}4)$$

a product that absorbs at 250 nm. Because all of the measurements were performed in water of neutral pH, and the UV absorption bands are of typical condensed-phase width for both $HO_2^\bullet$ and $O_2^{\bullet-}$, the resulting absorption was a sum of both $HO_2^\bullet$ and $O_2^{\bullet-}$ radicals. At elevated temperature, the fraction of $O_2^{\bullet-}$ in the measured signals is lower due to changes in equilibrium (eqs 4,-4) with increasing temperature.[16] Above 300 °C, the equilibrium lies almost entirely to the left, giving essentially only $HO_2^\bullet$.

Measurement of the reaction 1 rate under the chosen conditions is limited by the lowest oxygen concentration that can be applied before the oxygen is depleted by repeated electron pulses. However, with too high an oxygen concentration, the secondary reaction (5) becomes increasingly important as it

$$e_{aq}^- + O_2 \rightarrow O_2^{\bullet-} \quad (5)$$

generates $O_2^{\bullet-}$ without ever reacting with $H^\bullet$ atoms, thus obscuring the observed reaction 1 rate. Furthermore, it decreases the amount of H atoms produced by competition with reactions 2 and 3. The experimental limits placed on the O_2 concentration effectively minimized this pathway so that nearly all the e_{aq}^- were eventually converted to $H^\bullet$. To overcome the limitation of too low an O_2 concentration, the doses applied in the experiment were the lowest possible to obtain usable UV signals after averaging of 30 consecutive traces. However, even for the lowest applied doses, $H^\bullet$ atom recombination cannot be ignored in the overall reaction scheme. Reaction 6 slightly decreases the $H^\bullet$ atom concentration, especially at high doses due to its second-order nature. It becomes increasingly important at higher temperatures where this reaction becomes very fast.[17]

$$H^\bullet + H^\bullet \rightarrow H_2 \quad (6)$$

The collected UV traces were fitted to a complex water radiolysis model that includes a set of all the known water radiolysis reactions and all the extinction coefficients for species absorbing at the experimental wavelength. The occurrence of reaction 6 can be nicely accounted for when the dose dependence of the fitted kinetics is included. Therefore, all measurements were carried out using two different doses of roughly 2 and 10 Gy and at least three different oxygen concentrations.

Fits to the experimental data must take into account the relative dose delivered in each experiment, as well as changes in the absorbed radiation due to decreasing water density with increasing temperature. The relative dose delivered by the accelerator was measured by integrating charge on a thick brass "shutter" inserted between the beam port and sample cell. It is assumed that the absorbed dose is simply proportional to the water density, as long as the sample is thin enough to avoid severe scattering of the electrons. The water density was calculated using the IAPWS-IF97 formulation for light water PVT relations.[18]

III. Results and Analysis

The presence of more than one absorbing species ($HO_2^\bullet$, $O_2^{\bullet-}$, $OH^\bullet$, $H^\bullet$, etc.) reacting simultaneously leads to kinetically complex absorbance−time profiles that can only be resolved numerically using a computer code. In turn, this means that as many parameters as possible should be accurately known a priori; these include molar absorptivities of all species, *G* values, rate constants and radiation dose.

A. G Values. *G* values (escape yield of radicals in moles per unit energy of radiation absorbed) used in the data analysis were based on the compilation of previous measurements of Lin et al.,[19] and our unpublished results for the yields of hydrated electron, $H^\bullet$ atom, and H_2.[20] From the Lin et al. results we take the total yield $G(e_{aq}^- + OH^\bullet + H^\bullet)$ reported up to 350 °C and by subtraction of our experimental $G(H^\bullet) + G(e_{aq}^-)$ values we estimate $G(OH^\bullet)$ numbers in the studied temperature range. The *G* values for H_2O_2 and H_2 were based on previous data supplied by Elliot et al.[21,22]

B. Molar Absorption Coefficients. *OH*•. The product of ϵG for the $OH^\bullet$ radical in N_2O-saturated water was measured in our apparatus at constant dose at 230 and 250 nm for temperatures in the range 25−350 °C. Recombination in oxygen-free water is slow enough that a simple measurement of absorption at 200 ns after the 4 ns electron pulse is sufficient for this purpose. We confirmed previous observations that the $OH^\bullet$ radical spectrum does not change up to 200 °C[23] if a density correction is applied for the absorbed dose. However, considering the increase in the spur escape yields of initial transient species with temperature,[19] the absorption coefficient of $OH^\bullet$ radicals at 230 and 250 nm must become lower with temperature. This is apparently related either to the spectrum shifting toward deeper UV or to depleting of the 230 nm band with the temperature increase (more detailed analysis of the $OH^\bullet$ spectrum is the subject of a future paper[24]). Applying the measured ϵG and calculated $G(OH^\bullet)$ at a given temperature, the $OH^\bullet$ radical extinction coefficients for 230 and 250 nm have been determined. Figure 2 shows the temperature dependence of these parameters. The $OH^\bullet$ radical extinction coefficient continuously decreases with temperature from room temperature

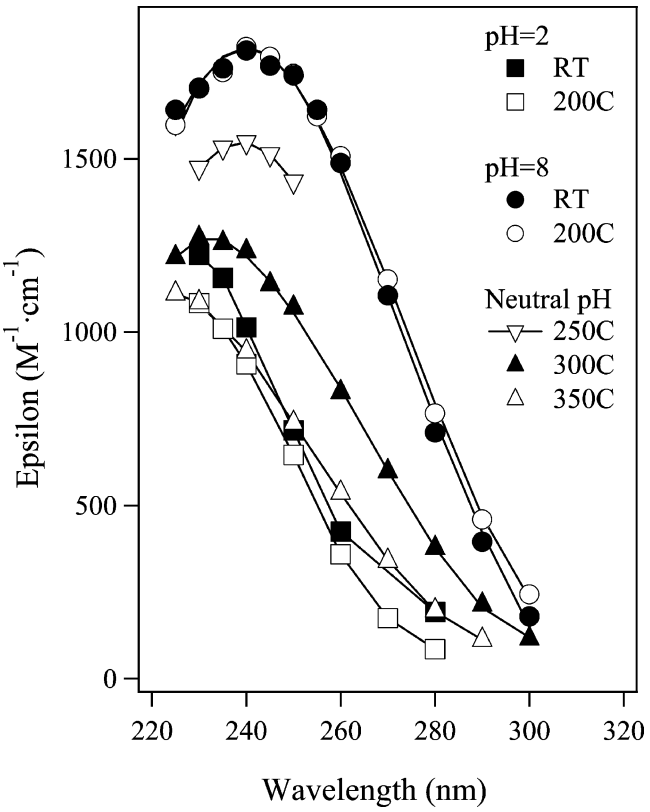

Figure 1. Temperature dependence of the $HO_2^{\bullet}/O_2^{\bullet-}$ radical spectrum at various pH. Circles: $O_2^{\bullet-}$ radicals at room temperature (solid) and 200 °C (open). Squares: $HO_2^{\bullet}$ radical at room temperature (solid) and 200 °C (open). Triangles: effective extinction coefficients of $HO_2^{\bullet}/O_2^{\bullet-}$ at 250 °C (inverse, open), 300 °C (solid), and 350 °C (open). All spectra shown were acquired using the same applied dose of 9.5 ± 0.5 Gy.

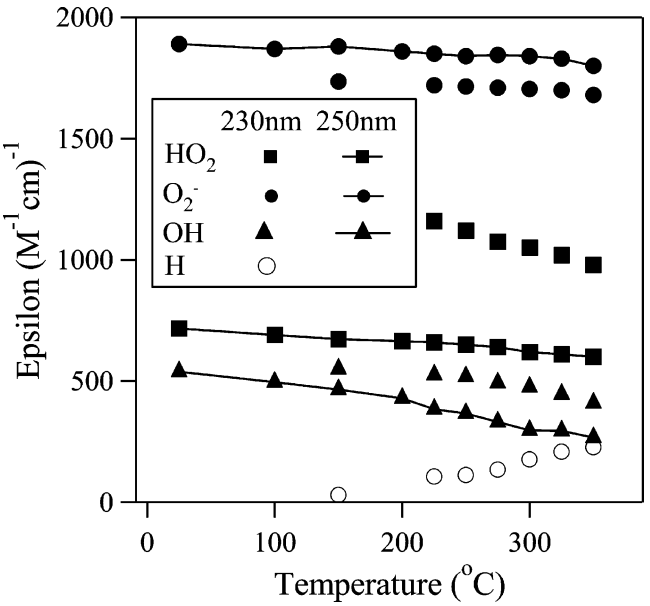

Figure 2. Changes of extinction coefficient of species contributing to the absorption at the experimentally chosen wavelengths. Symbols: extinction coefficients at 230 nm. Symbols and lines: extinction coefficients at 250 nm. Corresponding symbols: squares, $HO_2^{\bullet}$; filled circles, $O_2^{\bullet-}$; triangles, $OH^{\bullet}$; open circles, $H^{\bullet}$.

up to 350 °C. The values used for the data analysis are summarized in Table 1.

$HO_2^{\bullet}/O_2^{\bullet-}$. Initially, the molar absorptivities for $O_2^{\bullet-}$ and $HO_2^{\bullet}$ were determined on the basis of the $\epsilon_{max}G$ changes vs temperature reported by Christensen and Sehested up to 250 °C for hydrogenated and oxygenated solutions of variable pH.[16] To estimate the G values after the 1 μs electron pulse for these experimental conditions (i.e., H_2 and O_2 concentrations, and pH), we applied the total $G(e_{aq}^- + OH^{\bullet} + H^{\bullet})$ recently obtained from methyl viologen measurements by Lin et al.[19] However, from all our fitting attempts it was evident that the extinction coefficient values so derived for $HO_2^{\bullet}$and $O_2^{\bullet-}$ are too high. The increase of temperature implied an increase of the given extinction coefficients. Our kinetics observations indicate the opposite trend.

TABLE 1: Extinction Coefficients as a Function of Temperature (M^{-1} cm^{-1}) for the Species Experimentally Observed (n.d. = No Data Available)

			fit results (av values)					
	Christensen et al.		$HO_2^{\bullet}$		$O_2^{\bullet-}$		$OH^{\bullet}$	$H^{\bullet}$
temp (°C)	$HO_2^{\bullet}$ at λ_{max}	$O_2^{\bullet-}$ at λ_{max}	230 nm	250 nm	230 nm	250 nm	230 nm	230 nm
25	1251	1892	1222	717	1760	1890	582	20
100	1274	1950	n.d.	690	n.d.	1850	n.d.	n.d.
150	1290	1988	1183	673	1735	1813	550	30
200	1306	2027	n.d.	665	n.d.	1800	n.d.	n.d.
225	1314	2046	1160	660	1720	1750	525	106
250	1322	2066	1121	650	1715	1730	518	112
275	1330	2085	1075	640	1710	1700	492	134
300	1338	2105	1050	620	1705	1680	475	176
325	1346	2124	1020	610	1700	1660	445	208
350	1354	2143	980	600	1680	1600	409	227

Consequently, it was decided to record new $HO_2^{\bullet}$ and $O_2^{\bullet-}$ spectra as a function of temperature. Spectra were measured using a 50:50 mixture of H_2-pressurized water and O_2-saturated water, thus the final room-temperature concentrations of the H_2 and O_2 solutions upon mixing of the two solutions were approximately 5.0×10^{-2} and 6.5×10^{-4} *m*, respectively. To achieve acidic or basic pH, perchloric acid or potassium hydroxide were respectively added to the O_2-saturated water. Just as in the experiments of Christensen and Sehested,[16] the chemistry ensures that all the primary $OH^{\bullet}$, e^-_{aq}, and $H^{\bullet}$ radicals formed upon radiolysis are scavenged to form $HO_2^{\bullet}$ or $O_2^{\bullet-}$. The applied dose was held constant from day to day, varying on different days by no more than 6%. We were able to register $HO_2^{\bullet}$ spectra at pH = 2 and $O_2^{\bullet-}$ spectra at pH = 8 up to 200 °C. Figure 1 shows a comparison of $HO_2^{\bullet}$ and $O_2^{\bullet-}$ spectra collected at room temperature and at 200 °C. The extinction coefficients presented in Figure 1 represent the new experimental ϵG divided by $G(e_{aq}^- + OH^{\bullet} + H^{\bullet})$ obtained by Lin et al.[19] From the results presented in Figure 1 for the $HO_2^{\bullet}$ and $O_2^{\bullet-}$ spectra, one can see that a temperature increase up to 200 °C slightly lowers the $HO_2^{\bullet}$ extinction coefficient. This observation agrees with results obtained by Buxton et al., for $HO_2^{\bullet}/O_2^{\bullet-}$ spectra recorded up to 175 °C.[25] It also roughly agrees with the behavior of the gas-phase spectrum recorded by Kijewski and Troe.[26] In contrast, the $O_2^{\bullet-}$ spectrum does not change up to 200 °C within experimental error. Though these results contradict Buxton's report, it agrees with the observations of Christensen and Sehested[16] that the product $\epsilon_{max}G$ for $O_2^{\bullet-}$ increases more than for $HO_2^{\bullet}$ with increasing temperature. It should be noted, however, that the current result is quantitatively different from either of the previous reports.

Above 200 °C, reliable measurements could not be performed in acidic conditions as substantial corrosion in the metal flow system was observed. In addition, hot alkaline solution in the presence of oxygen etches the sapphire windows[27] and makes the UV measurements impossible due to excess light scattering.

Therefore, for temperatures higher than 200 °C, effective combined spectra of $HO_2^{\bullet}/O_2^{\bullet-}$ were recorded at neutral pH. The spectra recorded at 300 and 350 °C are shown in Figure 1 (triangles). The maximum of the $HO_2^{\bullet}/O_2^{\bullet-}$ effective spectrum at neutral pH shifts toward deeper UV and the effective extinction coefficients decrease with increasing temperature. The change in the effective $HO_2^{\bullet}/O_2^{\bullet-}$ spectrum can be correlated with the change of the pK_a value of the $HO_2^{\bullet}$ radical.

The value of the pK_a for equilibrium (4,−4) is 4.8 at room temperature[15] and increases to a value of 6.15 at 285 °C, according to the report of Christensen and Sehested.[16] Extrapolating these experimental numbers up to 350 °C, one can expect a value of p$K_a \sim 7$, which is above the pH of water at this temperature ($pH_{350°C} = 5.98$), thus suggesting predominance of $HO_2^{\bullet}$. For the whole range of temperatures between 200 and 350 °C, we have measured partial spectra of $HO_2^{\bullet}/O_2^{\bullet-}$ between 230 and 250 nm. A sample of a partial spectrum recorded at 250 °C is superimposed in Figure 1 (reversed triangles). The combined extinction coefficients obtained at 230 and 250 nm were used to estimate separate extinction coefficients for $HO_2^{\bullet}$ and $O_2^{\bullet-}$ at these wavelengths by iteration, using the ratio of $HO_2^{\bullet}$ and $O_2^{\bullet-}$ concentrations based on the pK_a value at a given temperature. For temperatures higher than 285 °C, the pK_a was extrapolated using a third-order polynomial function that fits the experimental pK_a values encountered at lower temperatures. Uncertainty in the extrapolated pK_a value is probably ±0.2 pK units at 350 °C. The iteration results were used as initial guesses in the analysis of the kinetics. During numerical analysis of the data, the initial guesses were slightly iterated to find the best fit. The measured combined absorbance applies in any case to the final product; separate extinction coefficients are only needed to fit the signal rise for relatively large O_2 concentrations, where the observed signal could be due, in part, to product contribution from reaction 5. The final best estimates of both extinction coefficients and their changes with the temperature are shown in Figure 2.

H•. The H• atom absorption spectrum was reported previously from room temperature up to 200 °C, and no changes in the spectral shape were found over this temperature range.[17] It is generally accepted that the absorption must be due to water molecules in the first solvation shell, because the hydrogen atom Lyman Alpha line is encountered far into the vacuum ultraviolet. The shape of the H• atom spectrum decreases exponentially toward the red and somewhat resembles the shape of the water absorption edge, which also does not change shape with temperature, although it shifts to the red.[28] (For water, the shape is probably controlled by the Franck−Condon envelope for the lowest bound-dissociative transition.[28]) At 250 nm, the H• atom extinction coefficient is as low as 30 M^{-1} cm^{-1}.[29,30] For our data analysis at 250 nm, the H• atom absorption was very minor. However, for all data recorded at 230 nm it was necessary to increase the value of the H• atom extinction coefficient, especially for temperatures higher than 200 °C. The changes of the H• atom extinction coefficient at 230 nm resulting from fits to the data are summarized in Table 1 and are superimposed in Figure 2. Given the 0.6 eV red shift of the water absorption edge between room temperature and 400 °C,[28] it seems quite reasonable to assume that the H• atom spectrum could shift by a similar amount.

H_2O_2 and e_{aq}^-. Both the hydrogen peroxide and the hydrated electron extinction coefficients were included in the data analysis and fits. However, they did not affect the fitted results as (i) the hydrated electron was converted to OH• radicals in tens of nanoseconds according to reaction 2, basically in the limit of our time resolution, and (ii) H_2O_2 forms in negligible amounts from OH• recombination during the course of the experiment due to strong scavenging of the radical by reaction 3, and could exist only as a product of spur reactions with much lower yields[22] and relatively small extinction coefficients in the range of interest.

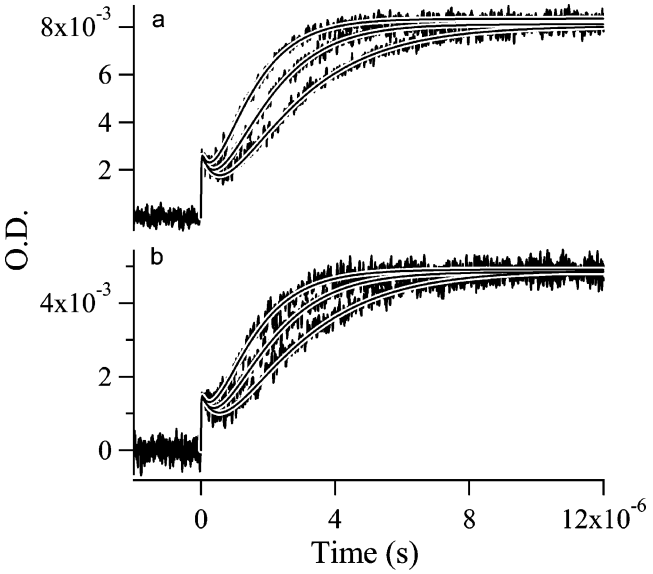

Figure 3. Formation of $HO_2^{\bullet}$ at 25 °C for two applied doses, (a) and (b), with (a) being a higher dose. The three traces of each set correspond to O_2 concentrations 3.2×10^{-5}, 6.5×10^{-5}, 1.3×10^{-4} *m*, respectively. The N_2O concentration varies between 1.18 and 1.00×10^{-2} *m*, and the H_2 concentration is a constant 4.82×10^{-2} *m*. Signals were acquired at 250 nm. Fits are superimposed as solid lines.

C. Data Analysis. For reaction 1, the change of the total absorbance with time after an electron pulse was initially measured for the given temperature range at 250 nm and neutral pH. A study was carried out as a function of temperature up to 350 °C. All data were collected at a pressure of 250 bar. Typical data taken at 25 and 200 °C are shown in Figures 3 and 4, with fitted curves superimposed. The signals track the initial decay of OH• radicals and subsequent formation of $HO_2^{\bullet}/O_2^{\bullet-}$ radicals by their absorption at 250 nm. The different sets of traces correspond to different doses applied, with larger amplitude signals representing the higher doses. The different traces correspond to different oxygen concentrations, where the concentration was varied between 1.6×10^{-5} and 1.3×10^{-4} *m*. The concentration of hydrogen was not changed for experiments conducted at a given temperature, and the concentration of nitrous oxide varied only by 20%, being kept in the range of 1.2×10^{-2} *m*. An increase of the oxygen concentration causes an apparent faster rise of the $HO_2^{\bullet}/O_2^{\bullet-}$ product, in agreement with pseudo-first-order behavior. At temperatures above 200 °C, the signal amplitude at 250 nm decreases considerably (compare absorption spectra in Figure 1) for the range of applied doses. An increase of the dose at higher temperatures causes two unwanted effects: (i) increase of contributions from second-order reactions and (ii) depletion of the oxygen in the system as a result of the many electron pulses applied to the same sample. Therefore, the experiment was repeated for the range of temperatures 150−350 °C at 230 nm where there is a much higher contribution from the $HO_2^{\bullet}$ absorption than from $O_2^{\bullet-}$, and higher overall effective absorption. Using these conditions, we could keep the same range of applied doses for all the desired temperatures.

The simple pseudo-first-order approach to the kinetics was not good enough to provide satisfactory fits to the data. We

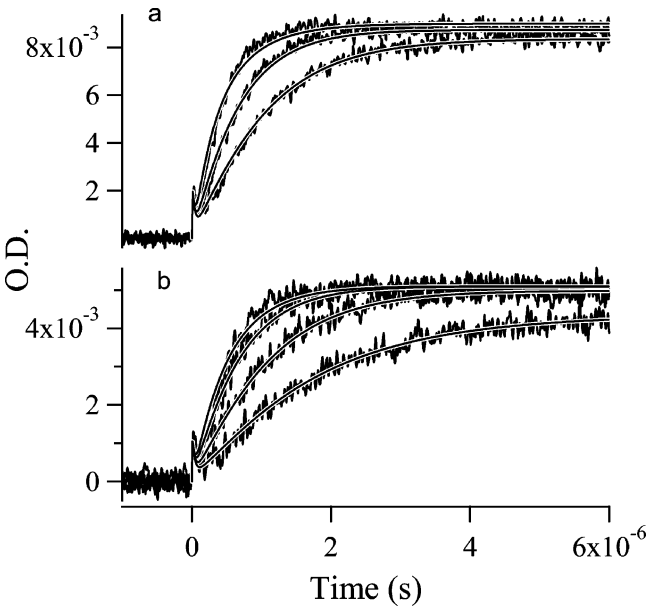

Figure 4. Formation of $HO_2^•$ at 200 °C and two applied doses (a) and (b), with (a) being a higher dose. The four traces at each dose correspond to following O_2 concentrations 1.625×10^{-5}, 3.25×10^{-5}, 6.5×10^{-4}, 1.3×10^{-4} M, where the higher the concentration, the faster the observed rise rate. Here, the N_2O concentration varies between 1.00 and 1.18×10^{-2} *m*, and the H_2 concentration is 4.82×10^{-2} M. The signals are acquired at 250 nm. Fits are superimposed as solid lines.

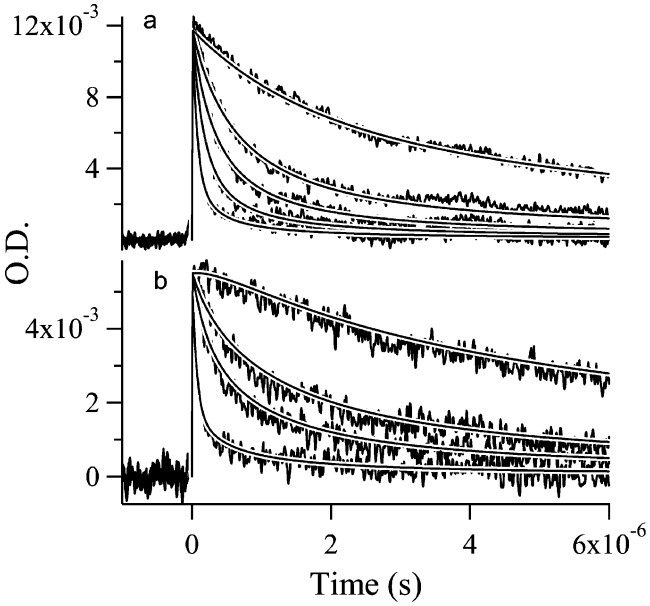

Figure 5. Decay of the $OH^•$ absorption after addition of H_2 at 350 °C for two applied doses (a = 8.5 Gy, b = 17 Gy). H_2 concentrations: (a) 0.0, 3.55×10^{-3}, 7.16×10^{-3}, 3.52×10^{-2} *m*; (b) 0.0, 3.55×10^{-3}, 7.16×10^{-3}, 1.42×10^{-2}, 3.52×10^{-2} *m*. A faster decay corresponds to higher H_2 concentration. The N_2O concentration varies between 2.5 and 1.28×10^{-2} *m*. The signals were acquired at 250 nm. Fits are superimposed as solid lines.

were forced to build a kinetically complex model that included many reactions involving all reactive species present. The observed kinetics can be modeled by a set of some 50 reactions, using a model described in previous publications,[6] but adapted to handle UV-absorbing species. Each rate constant in the model was tested for sensitivity toward the fit quality. The majority of the reactions are only minor contributors to the kinetics and can be ignored. The set of reactions responsible for the observed kinetics follows:

$$e_{aq}^- + N_2O \rightarrow OH^• + N_2 \quad (2)$$

$$OH^• + H_2 \rightarrow H^• + H_2O \quad (3)$$

$$H^• + O_2 \rightarrow HO_2 \quad (1)$$

$$HO_2^• \leftrightarrow O_2^{•-} + H^+ \quad (4,-4)$$

$$H^• + H^• \rightarrow H_2 \quad (6)$$

$$H^• + N_2O \rightarrow OH^• + N_2 \quad (7)$$

$$H^• + O_2^{•-} \rightarrow HO_2^- \quad (8)$$

$$H^• + HO_2^• \rightarrow H_2O_2 \quad (9)$$

The temperature dependence of reaction 2 was previously determined[31] and was fixed for the data fitting.

Non-Arrhenius behavior of k_3 was reported previously[13] and these results were used up to 325 °C. However, at 350 °C a satisfactory fit could not be achieved with the rate constant value reported previously.[13] It appeared that the reported value was significantly lower than was necessary to fit the present experimental results. To redetermine k_3 at 350 °C, an experiment was performed to directly monitor the $OH^•$ radical decay at 250 nm in the presence of N_2O and various concentrations of H_2, but in the absence of O_2. With these reactants present, the e^-_{aq} are scavenged by the N_2O and converted to $OH^•$. The $OH^•$ subsequently reacts via reaction 3. To fit the experimental traces, we used the same fitting model described above, but k_3 was fitted instead of k_1. The results of this experiment are presented in Figure 5. With increasing H_2 concentrations, a faster decay of the $OH^•$ radical is observed as a result of reaction 3. However, at the same time, reaction 7 restores part of the $OH^•$ radicals, giving a contribution to the absorption in the tail of the signal (a chain reduction of the N_2O). For the highest concentration of H_2, the contribution of reaction 7 is less obvious, as the regenerated $OH^•$ is quickly removed again by reaction 3. The $H^•$ atom does not absorb significantly at this wavelength, and its second-order decay rate via reaction 6 is diffusion-limited. From the fits, a k_3 value of $(6.0 \pm 0.5) \times 10^8$ M^{-1} s^{-1} was obtained, which is roughly 70% higher than the rate reported previously. (We should note that the previous value was obtained at the detection limit of the competition method being used, and a large error bar was admitted.[13]) The fits were found to have a high sensitivity to k_7. It was found that the collected traces could be fit only using rate constant values between 1.0 and 1.5×10^8 M^{-1} s^{-1} to give an uncertainty in k_3 of $\pm 0.5 \times 10^8$ M^{-1} s^{-1}. Therefore, the upper limit for k_7 was taken to be 1.5×10^8 M^{-1} s^{-1} at 350 °C. On the basis of the reported room-temperature rate constant[32] of 2.1×10^6 M^{-1} s^{-1}, we estimated the Arrhenius dependence for reaction 7 with the activation energy E_a = 18.5 kJ mol^{-1} and pre-exponential $A = 3.7 \times 10^9$ M^{-1} s^{-1} over the temperature range studied. Corresponding rate constants for reaction 7 at given temperatures were included in the reaction 1 analysis as a minor correction.

Values for k_{-4} were calculated assuming diffusion-limited behavior on the basis of the Debye−Smoluchowski equation

$$k_{diff} = \beta 4\pi RDF_D \quad (10)$$

with

$$F_D = \frac{\delta}{e^{\delta-1}}, \delta = \frac{z_a z_b e^2}{4\pi\epsilon_0 \epsilon R k_B T}$$

where k_{diff} is written as the Smoluchowski rate times the Debye factor, F_D. The value of e in the definition of δ is the fundamental electron charge, z_a and z_b are the formal charges of the reactants, $D = D_a + D_b$ is the relative diffusion coefficient of reactant ions a and b, R is the reaction encounter distance, k_B is Boltzmann's constant, ϵ_0 is the permittivity of free space, ϵ is the dielectric constant, and β is a statistical factor to account for spin effects (equal to 1 in this case). The reaction rate was scaled with temperature as proposed previously by Elliot.[6] k_4 was determined using K_a numbers for $HO_2^\bullet$ radicals reported by Christensen and Sehested,[16] together with the calculated values of the reverse reaction (−4).

The reaction 6 rate constant was previously determined up to 275 °C by Sehested and Christensen,[17] and we were able to extrapolate it up to 350 °C without any dramatic effect on the fit results, suggesting that this reaction follows Arrhenius behavior up to 350 °C. There is some uncertainty about these numbers, as the authors (correctly) reported experimental values of $2k/\epsilon$ but further assumed that the $H^\bullet$ atom extinction coefficient was constant with temperature. The present data analysis indicates that there is an increase of the $H^\bullet$ atom extinction coefficient with increasing temperature, especially at shorter wavelengths. It would imply that the $2k$ numbers reported by Sehested and Christensen represent a lower limit for this rate constant. In our analysis, we tested the sensitivity of the fits by varying this rate constant by ±30%. For the highest values used, we obtained only 5% higher values for the reaction 1 rate constant, suggesting that our results are only slightly affected by any uncertainty in the reaction 6 rate constant.

Values for k_9 as a function of temperature were reported previously[33] up to 149 °C. To our knowledge, reaction 8 has never been studied above room temperature. Following the example of Elliot,[6] we set k_8 equal to k_9. Neither reaction is important to the present analysis for temperatures below 200 °C. However, for higher temperatures it was important to reduce the extrapolated value of k_9 (see below).

An Arrhenius plot of the fitted k_1 values is shown in Figure 6, and the rate constants are given in Table 2. Data were fitted globally for 3−5 oxygen concentrations and two doses. Thus, a global fit was obtained for 6−10 single experiments at each temperature. As stated above, sensitivities to various estimated parameters and different starting values were tested by multiple least-squares minimizations. The error bars are indicative of the range of rate constants obtained when the fit was "good", but this is a qualitative rather than a quantitative measure. The line in the figure is Elliot's extrapolation[6] of the Noyes equation (11) fit to the previously available data obtained from room temperature up to 200 °C:

$$k_{obs}^{-1} = k_{diff}^{-1} + k_{act}^{-1} \quad (11)$$

where rate constant, k_{act}, was calculated on the basis of Arrhenius equation

$$k_{act} = Ae^{-E_a/RT} \quad (12)$$

with the parameters $E_a = 7.75$ kJ mol^{-1} and $A = 5.71 \times 10^{11}$ M^{-1} s^{-1}, and k_{diff} is defined by eq 10 with $F_D = 1$, as the reactants are non-ionic. Within error limits, our data agree with previous reports[6−8] up to 100 °C but then undershoot the extrapolation at higher temperatures. Above 300 °C, the fitted rate constant actually decreases. At 350 °C, the rate constant is more than a factor of 2.5 below the extrapolation of Elliot.[6] (Note that we do not advocate an Arrhenius form for k_{act} in general, as should be made clear below.)

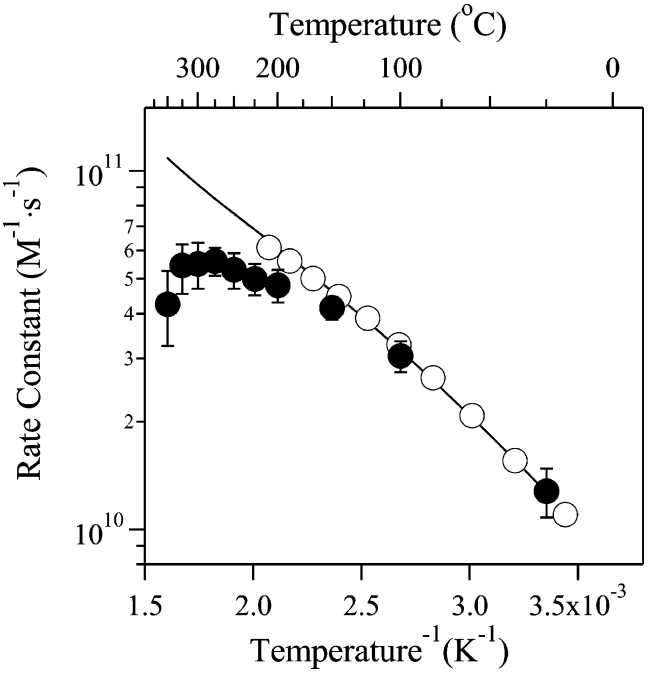

Figure 6. Arrhenius plot for reaction 1 (solid circles). The open circles represent previously reported data available up to 200 °C,[8] and the solid line represents their Arrhenius extrapolation to higher temperatures.

TABLE 2: Fitted Rate Constants (M^{-1} s^{-1}) for Reactions 1, 9, and 14[a]

	$k_1 \times 10^{-10}$			
temp (°C)		using rxn 14	$k_9 \times 10^{-10}$	$k_{14} \times 10^{-10}$
25	1.25	n.d.	0.96	n.d.
100	2.9	n.d.	3.6	n.d.
150	3.8	4.1	7.5	1.00
200	4.46	4.90	8.5	7.55
225	4.78	5.12	5.8	10.6
250	5.3	5.30	3.6	16.5
275	5.4	5.81	2.4	18.1
300	5.7	6.11	2.4	23.7
325	5.5	6.42	1.6	26.0
350	5.0	6.49	1.0	28.0

[a] Two columns of values are shown for k_1, where the first column shows results from fits performed without reaction 14, and the second column includes it in the fitting model. n.d. = no data available.

Figure 7 shows changes in k_9 as a function of temperature. These data also demonstrate non-Arrhenius behavior that is even more extreme than for reaction 1. The effect of reaction 9 at high temperature was very obvious as its rate affects both the time profile and the final amplitude of the $HO_2^\bullet/O_2^{\bullet-}$ product absorption, therefore affecting the fitted k_1 value. We have no disagreement with the previous measurements by Lundstrom et al.,[33] up to 150 °C. In this range of temperatures, reaction 9 is of little importance because the $O_2^{\bullet-}$ absorption prevails. We assumed Arrhenius behavior for reaction 8, using parameters suggested by Elliot[6] over the entire temperature range studied. In fact, neither reaction 8 nor 9 was very important below 200 °C. Above 200 °C, it was necessary to decrease the value for k_9 in comparison to the Arrhenius behavior reported previously.[33] Above 225 °C, k_9 even started to decrease. The solid circles in Figure 7 represent the values obtained from this

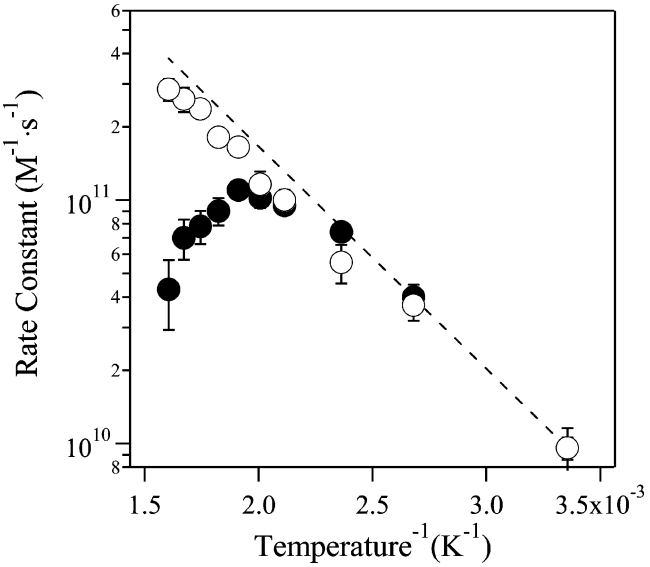

Figure 7. Arrhenius plot for reaction 9 (solid circles) and alternative reaction 14 (open circles). The dashed line represents Arrhenius extrapolation of previously reported data for reaction 9 available up to 150 °C to higher temperatures.

analysis. As one can see, the reaction rate constant decreases dramatically with increasing temperature, and above 300 °C, the reaction is not required. The numbers plotted in Figure 7 represent upper limits for this rate constant.

IV. Discussion

The discovery that reaction 1 is not diffusion-limited in high-temperature water comes as a surprise, given that there is no barrier to O−H bond formation in the gas phase. Both species are hydrophobic, so there is no reason to expect a strong perturbation of the water solvent on either reactant, or particular involvement of a water molecule in the transition state. Standard ab initio density functional calculations confirm that the reaction path is essentially unaffected by a dielectric continuum environment, though the product $HO_2^\bullet$ radical is stabilized by solvation and hydrogen bonding.[34] However, to say that there is no barrier to the reaction is incorrect, because there are large barriers in the potential for approach of the $H^\bullet$ atom at 0° or 90° with respect to the O−O axis. Only for an approach along roughly 45° is there no barrier.[3] Thus, in expecting a diffusion-limited reaction rate, we were assuming that the solvent cage effect would provide sufficient angular averaging in recollisions so that the proper angle of approach would always be found. This is apparently not the case because of the very high diffusion rates of both reactants at high temperatures.

We can use eq 11 to interpolate between the diffusion limit and a barrier-limited reaction rate. Because of the presence of two "spin-active" reactants, the spin statistical factor, β, in eq 10 now necessitates consideration.[35] In the present case of a doublet H atom reacting with a triplet O_2 molecule we could expect one-third of initial encounter pairs to be reactive doublets $|D(\pm 1/2)\rangle$, and two-thirds to be unreactive quartet $|Q(\pm 1/2)\rangle$, $|Q(\pm 3/2)\rangle$ states. But the presence of zero field splitting in the triplet O_2 molecule means that doublet and quartet are not true eigenstates of the encounter pair spin Hamiltonian, and the doublet/quartet character will oscillate in time. Spin quantization along the O−O axis is conserved, but the $|Q(\pm 1/2)\rangle$ sublevels mix with the $|D(\pm 1/2)\rangle$ sublevels. The $|Q(\pm 3/2)\rangle$ sublevels do not mix and remain unreactive. Solution of the time-dependent Schrödinger equation and substitution of the O_2 zero field

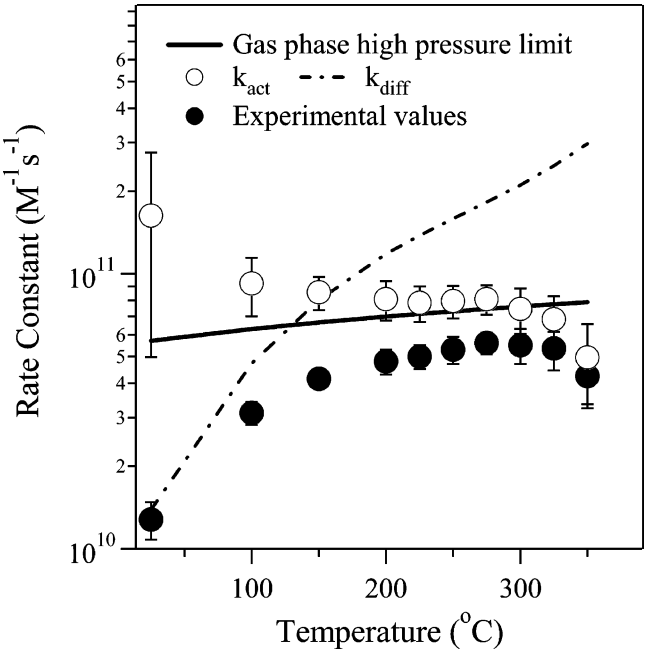

Figure 8. Comparison of experimental results of k_1 (solid circles) with the high-pressure limit data[1] (solid line) and k_{diff} determined from eq 10 with $\beta(T)$ calculated from eq 13. Open circles represent values of k_{act} inferred from the Noyes equation.

splitting magnitude produces a 7.6 ps oscillation period,[35] which means that the reaction probability will oscillate on the time scale of a diffusive encounter. This problem of an oscillatory reaction probability during a diffusive encounter has been solved by Green et al.,[36] who provide the solution

$$\beta = \frac{2}{3}\left[\frac{1 + R\sqrt{\omega/D}}{2 + R\sqrt{\omega/D}}\right] \tag{13}$$

where ω is 2π divided by the oscillation period. The 2/3 prefactor removes from consideration the unreactive $|Q(\pm 3/2)\rangle$ spin states. Thus, the value of β will lie between 1/3 and 2/3 depending on the diffusion rate, and therefore the temperature.

In Figure 8 we plot our measured rate constants and the estimated diffusion limit based on eq 10. The diffusion coefficient for O_2 is 2.4×10^{-9} m^2 s^{-1} at 25 °C[37] and the $H^\bullet$ atom diffusion coefficient is 7.5×10^{-9} m^2 s^{-1}.[38] We estimate the higher-temperature diffusion rates by scaling with T/viscosity, as suggested by Stokes−Einstein behavior. Equation 13 yields a spin factor closer to 2/3 than to 1/3 for the entire temperature range. With this estimate of the diffusion limit, the activated barrier reaction rate k_{act} is deduced from the Noyes equation as the open circles in Figure 8. The rate constant k_{act} is the rate of reaction that would apply if diffusional transport were no constraint.[39] As we expected, the reaction is nearly diffusion-limited at room temperature but is almost entirely limited by some barrier above 200 °C.

According to classical statistical mechanics, the (Maxwell−Boltzmann) velocity distribution function for collisions of the two reactants in a solvent will be exactly the same as in gas-phase collisions of the same molecules. Then the overall reaction probability per collision will also be the same, if the solvent does not modify the potential surfaces.[40] The appropriate gas-phase quantity for comparison is the so-called high-pressure limiting rate constant, where a third body is always available to carry away or supply excess energy.[39] The high-pressure limit for $H^\bullet + O_2$ has been estimated by extrapolation of pressure

falloff behavior by Troe and co-workers,[1,41] and calculated with high level ab initio methods by Harding et al.[3] Their high-pressure gas-phase limit for this reaction is also plotted as the solid line in Figure 8. Thus our measured aqueous-phase rate constants are in virtually perfect agreement with the calculated high-pressure limit between 200 and 300 °C.

Although we can justify equivalent reaction probability per collision in this case by the hydrophobic nature of the reactants (i.e., the entrance channel for reaction is hardly perturbed), it is also necessary to have equivalent encounter frequency in both liquid and gas phase to obtain the same reaction rates. The general picture is that solvent caging produces many collisions and recollisions within a short time, separated by very long periods of solvent isolation of the reactants. But the time averaged number of collisions is nearly the same in both phases. If we identify a "collision" by the contact distance between reactants, then to a first approximation the relative probability (or volume density) of collisions can be obtained by comparing H...O_2 radial distribution functions $g(r)$ for the dense fluid and the dilute gas at the contact distance R. It is well-established that for small hydrophobic species in water molecular dynamics simulations, the short-range solute−solute radial distribution functions deviate very little from unity (the dilute gas limit).[42,43] Even so, we find the agreement between our aqueous-phase result and the calculated high-pressure limit of ref 3 to be remarkably good.

Below 200 °C the value of k_{act} is apparently larger than the gas-phase high-pressure rate. Although there is large error in the estimate of k_{act} at room temperature where k_{diff} dominates, a larger value of the reaction rate in water relative to gas phase might be expected on the basis of the phenomenon of "hydrophobic attraction".[44] When both hydrophobes are confined within the same solvent cage, some of the unfavorable solvation free energy of the reactants is recovered. This means that the actual number of collisions of H and O_2 is larger in water than in the gas phase, and the $g(R)$ "at contact" for H...O_2 will be slightly larger than unity. The hydrophobic acceleration of the rate is expected to be more pronounced at low temperature,[13,44] consistent with the behavior of k_{act} in Figure 8. However, the apparent (3x) hydrophobic acceleration would imply an association free energy on the order of kT. This is probably too large to be consistent with the extreme linearity of Henry's law constants for small hydrophobic gas molecules like O_2.[45,46]

There is a small discrepancy for the data points above 300 °C, in that we have no mechanism to explain the apparent slight decrease in rate constants. However, attention should be given to the larger error bars in these data points. Numerous uncertainties exist in the fitting of these data. The pK_a for the $HO_2^{\bullet}/O_2^{\bullet-}$ system is not actually known, nor are the actual separate extinction coefficients for these species. The rate of approach to equilibrium has an effect on the fitting. In addition, there is the issue of actual oxygen concentration in the experiments. We flow a mixture of O_2- and H_2-saturated water through metal tubing at high temperature. It could well be that we reduce a fraction of the O_2 on the way into our radiolysis cell. In this case, the fitted rate constants will be low due to the error in concentrations. Still another explanation is discussed below in the context of the $H^{\bullet} + HO_2^{\bullet}$ cross reaction. Given all of these uncertainties of the highest-temperature points, and the superb agreement with the high-pressure limit at lower temperatures, we advise use of the high-pressure limit rate constant in water above 300 °C as well.

The results of our study of the $H^{\bullet} + O_2$ reaction confirm to a large extent the analysis of high-temperature muonium rate constants made by Percival and co-workers.[47,48] They studied several different reactions of muonium "atom" with aromatic systems, both diffusion-limited and non-diffusion-limited, and also spin exchange with Ni^{2+} ion. In nearly all cases they found a decrease or plateau in apparent reaction rate above 250 °C and decided that the common thread was the decrease of collision frequencies per encounter because of the increased diffusion rate and reduced caging effect. A number of other free radical reactions involving $OH^{\bullet}$ radicals, $H^{\bullet}$ atoms, and e^-_{aq} are known to be diffusion-limited near room temperature but deviate from the diffusion limit in hot pressurized water.[8] On the basis of their analysis of collision frequencies, Percival and co-workers suggested[49] this should be a general theme of virtually all of the small free radicals involved in water radiation chemistry.[50]

As we now consider the behavior of reaction 9 as illustrated in Figure 7, we can appreciate that there probably is a strong orientational preference for the reaction to form hydrogen peroxide. At room temperature, the rate constant is at least near the diffusion limit. The fast diffusion of the $H^{\bullet}$ atom may contribute to the slowing of the reaction at higher temperature, causing the rate to reach a "high-pressure limit." Unlike the $H^{\bullet} + O_2$ case, the hydroperoxyl radical should be hydrogen bonded, and this might strongly affect the potential and the orientational averaging, to change the nature of the reaction relative to the gas phase. However, the magnitude of the rate constant decrease shown in Figure 7 is difficult to rationalize.

In the gas phase, reaction 9 is practically not observed and the result of $H^{\bullet}$ atom reaction with $HO_2^{\bullet}$ leads to products via three different reaction channels (13)−(15). Among all channels,

$$H^{\bullet} + HO_2^{\bullet} \rightarrow H_2 + O_2 \quad (13)$$

$$H^{\bullet} + HO_2^{\bullet} \rightarrow 2OH^{\bullet} \quad (14)$$

$$H^{\bullet} + HO_2^{\bullet} \rightarrow H_2O + O^{\bullet} \quad (15)$$

reaction 14 was found to contribute more than 90% in the $H^{\bullet} + HO_2^{\bullet}$ process at room temperature.[51−54] Reaction 13 would be nearly indistinguishable from reaction 9 in our experiment, and the oxygen atom product of reaction 15 would react with water to form peroxide, making it kinetically equivalent to reaction 9. To our knowledge, reaction 14 was never reported in the condensed phase. We decided to extend the reaction set by addition of reaction 14 and refit our data. The k_1 value was constrained to be equal to the gas-phase high-pressure limit as suggested above (i.e., k_{act} was constrained). The results of the fitting for reaction 14 are included in Figure 7 as open circles. The fit is good, giving an Arrhenius activation energy $E_a = 16.3$ kJ mol^{-1} and preexponential $A = 6.6 \times 10^{12}$ M^{-1} s^{-1} for reaction 14.

As reaction 14 recreates the initial substrate (i.e., the $H^{\bullet}$ atom via reaction 3), the oxygen uptake in 30 consecutive and averaged electron shots is much larger than one would expect from only reaction 1. It would cause a gradual decrease in the apparent risetime of $HO_2^{\bullet}$ signal after each consecutive electron shot for the lowest oxygen concentration used in the experiment. Indeed we observed such an effect, especially above 300 °C. Initially, we thought that it was caused by the reactions on the metal walls in our high-temperature preheater/cell system. However, it can also be explained by the occurrence of the chain reaction where concentration of $HO_2^{\bullet}$ and the $H^{\bullet}$ atom are suitable to propagate the chain at the lowest O_2 concentration. That is the only positive evidence for reaction 14 in our system.

On the other hand, there is no proof that reaction 9 is present in our system either. In the presence of reaction 14, the rate of reaction 9 was varied between 1.0 and 5.0 $\times$ 10^{10} M^{-1} s^{-1}, showing no important effect on the analysis, but the fitting was slightly better where the reaction 9 rate was kept at the lower end. It is not the intention of this work to prove or disprove whether reaction 9 or 14 is the predominant channel for the $H^\bullet + HO_2^\bullet$ process in aqueous solution, as both lead to a similar answer about the reaction 1 temperature dependence. Nevertheless, the model including reaction 14 removes the inexplicable decrease in rate at elevated temperature for both reactions 1 and 9, provides reasonable numbers for the reaction 14 rate constant, and is consistent with gas-phase data. It should be strongly considered in future experiments and modeling.

IV. Summary

This work has yielded measurements of the reaction rate of $H^\bullet$ atom with O_2 in pressurized water up to 350 °C and allows one of the first direct comparisons of a free radical association reaction in water with the corresponding gas-phase reaction over a wide temperature range. Perhaps not surprisingly because of the hydrophobic character of the reactants, the aqueous-phase rate constants agree very well with the gas-phase high-pressure limit once diffusion-limit effects are removed. On the other hand, it has not been generally recognized in the past that the rate of diffusion-limited radical reactions in water may plateau or even decrease at temperatures above 200 °C.[49] It has been implicitly assumed that solvent caging would remain effective to much higher temperature. Therefore, this work has major implications for modeling of free radical processes in water, such as in nuclear reactors or supercritical water oxidation systems.

Acknowledgment. We thank Dr. Sergey Chemerisov for maintaining and operating the linac used in this work. We thank Dr. Daniel M. Chipman at the Notre Dame Radiation Laboratory for his density functional calculation of the $H + O_2$ reaction channel under the dielectric continuum approximation. We thank Dr. Chipman as well as Dr. Larry Harding at Argonne National Laboratory, and Dr. Nick Green of Oxford University for useful conversations. Work at Argonne National Laboratory was performed under the auspices of the Office of Science, Division of Chemical Science, US-DOE under contract number W-31-109-ENG-38. Additional support has been provided by US-DOE NERI grant 02-060. The Notre Dame Radiation Laboratory is supported by the Office of Basic Energy Sciences at the United States Department of Energy. This is document number NDRL-4675 from the Notre Dame Radiation Laboratory.

References and Notes

(1) Hahn, J. K., L.; Luther, K.; Troe, J. *Phys. Chem. Chem. Phys.* **2004**, *6*, 1997.

(2) Baulch, D. L.; Bowman, C. T.; Cobos, C. J.; Cox, R. A.; Just, T.; Kerr, J. A.; Pilling, M. J.; Stocker, D.; Troe, J.; Tsang, W.; Walker, R. W.; Warnatz, J. *J. Phys. Chem. Ref. Data* **2005**, *34*, 757.

(3) Harding, L. B.; Troe, J.; Ushakov, V. G. *Phys. Chem. Chem. Phys.* **2000**, *2*, 631.

(4) Brock, E. E.; Savage, P. E. *AIChE J.* **1995**, *41*, 1874.

(5) Macdonald, D. D. *Corrosion* **1992**, *48*, 194.

(6) Elliot, A. J. *Report AECL-11658* **1996**.

(7) Elliot, A. J. *Radiat. Phys. Chem.* **1989**, *34*, 753.

(8) Elliot, A. J.; McCracken, D. R.; Buxton, G. V.; Wood, N. D. *J. Chem. Soc. Faraday Trans.* **1990**, *86*, 1539.

(9) Roduner, E.; Tregennapiggott, P. L. W.; Dilger, H.; Ehrensberger, K.; Senba, M. *J. Chem. Soc., Faraday Trans.* **1995**, *91*, 1935.

(10) Takahashi, K.; Cline, J. A.; Bartels, D. M.; Jonah, C. D. *Rev. Sci. Instrum.* **2000**, *71*, 3345.

(11) Takahashi, K.; Bartels, D. M.; Cline, J. A.; Jonah, C. D. *Chem. Phys. Lett.* **2002**, *357*, 358.

(12) Williams, D. D.; Blachly, C. H.; Miller, R. R. *Anal. Chem.* **1952**, *24*, 1819.

(13) Marin, T. W.; Jonah, C. D.; Bartels, D. M. *Chem. Phys. Lett.* **2003**, *371*, 144.

(14) Wiebe, R.; Gaddy, V. L. *J. Am. Chem. Soc.* **1934**, *56*, 76.

(15) Bielski, B. H. J.; Cabelli, D. E.; Arudi, R. L.; Ross, A. B. *J. Phys. Chem. Ref. Data* **1985**, *14*, 1041.

(16) Christensen, H.; Sehested, K. *J. Phys. Chem.* **1988**, *92*, 3007.

(17) Sehested, K.; Christensen, H. *Radiat. Phys. Chem.* **1990**, *36*, 499.

(18) Wagner, W.; Kruse, A. *Properties of Water and Steam: The Industrial Standard IAPWS-IF97 for the Thermodynamic Properties of Water*; Springer: Berlin, 1998.

(19) Lin, M. Z.; Katsumura, Y.; Muroya, Y.; He, H.; Wu, G. Z.; Han, Z. H.; Miyazaki, T.; Kudo, H. *J. Phys. Chem. A* **2004**, *108*, 8287.

(20) Janik, D.; Janik, I.; Bartels, D. M. *J. Phys. Chem.*, manuscript in preparation.

(21) Elliot, A. J.; Chenier, M. P.; Ouellette, D. C. *Can. J. Chem.-Rev. Can. Chim.* **1990**, *68*, 712.

(22) Elliot, A. J.; Chenier, M. P.; Ouellette, D. C. *J. Chem. Soc., Faraday Trans.* **1993**, *89*, 1193.

(23) Elliot, A. J.; Buxton, G. V. *J. Chem. Soc., Faraday Trans.* **1992**, *88*, 2465.

(24) Janik, I.; Bartels, D. M.; Jonah, C. D. *J. Phys. Chem.*, submitted.

(25) Buxton, G. V.; Wood, N. D.; Dyster, S. *J. Chem. Soc., Faraday Trans. 1* **1988**, *84*, 1113.

(26) Kijewski, H.; Troe, J. *Helv. Chim. Acta* **1972**, *55*, 205.

(27) Walther, J. V. *Geochim. Cosmochim. Acta* **1997**, *61*, 4955.

(28) Marin, T. W.; Takahashi, K.; Bartels, D. M. *J. Chem. Phys.* **2006**, *125*, 104314.

(29) Nielsen, S. O.; Michael, B. D.; Hart, E. J. *J. Phys. Chem.* **1976**, *80*, 2482.

(30) Janata, E. *Proc. Indian Acad. Sci. Chem. Sci.* **2002**, *114*, 731.

(31) Takahashi, K. J.; Ohgami, S.; Koyama, Y.; Sawamura, S.; Marin, T. W.; Bartels, D. M.; Jonah, C. D. *Chem. Phys. Lett.* **2004**, *383*, 445.

(32) Czapski, G.; Bielski, B. H. J. *Radiat. Phys. Chem.* **1993**, *41*, 503.

(33) Lundstrom, T.; Christensen, H.; Sehested, K. *Radiat. Phys. Chem.* **2004**, *69*, 211.

(34) Chipman, D. M. Unpublished work, 2006.

(35) Schmidt, K. H.; Han, P.; Bartels, D. M. *J. Phys. Chem.* **1995**, *99*, 10530.

(36) Green, N. J. B.; SpencerSmith, R. D.; Rickerby, A. G. *Chem. Phys.* **1996**, *212*, 99.

(37) Han, P.; Bartels, D. M. *J. Phys. Chem.* **1996**, *100*, 5597.

(38) Benderski, W. A.; Krivenko, A. G.; Rukin, A. N. *Chim. Vysok. Energ.* **1980**, *14*, 400.

(39) Pilling, M. J.; Seakins, P. W. *Reaction Kinetics*; Oxford University Press: Oxford, U.K., 1995.

(40) For the purpose of qualitative discussion here we consider the reaction rate to be a product of collision frequency and reaction probability per collision. More rigorous treatments as in ref 3 consider in detail the conversion of translational degrees of freedom into rotational modes of the product. The capture probability becomes a function of the energy and the angular momentum *J*, so that the "collision radius" can only be defined in terms of a distribution. The point here is that this distribution should be the same regardless of third body density, so long as the dense fluid does not change the binary interaction potential of the reactants.

(41) Cobos, C. J.; Hippler, H.; Troe, J. *J. Phys. Chem.* **1985**, *89*, 342.

(42) Smith, D. E.; Haymet, A. D. J. *J. Chem. Phys.* **1993**, *98*, 6445.

(43) Matubayasi, N.; Nakahara, N. *J. Phys. Chem. B* **2000**, *104*, 10352.

(44) Roduner, E.; Bartels, D. M. *Ber. Bunsen-Ges. Phys. Chem.* **1992**, *96*, 1037.

(45) Wilhelm, E.; Battino, R.; Wilcock, R. J. *Chem. Rev.* **1977**, *77*, 219.

(46) Battino, R.; Clever, H. L. *Chem. Rev.* **1966**, *66*, 395.

(47) Ghandi, K.; Addison-Jones, B.; Brodovitch, J. C.; Kecman, S.; McKenzie, I.; Percival, P. W. *Physica B (Amsterdam)* **2003**, *326*, 55.

(48) Ghandi, K.; Addison-Jones, B.; Brodovitch, J. C.; McKenzie, I.; Percival, P. W.; Schuth, J. *Phys. Chem. Chem. Phys.* **2002**, *4*, 586.

(49) Ghandi, K.; Percival, P. W. *J. Phys. Chem. A* **2003**, *107*, 3005.

(50) On this point we agree with Percival and co-workers for those recombination reactions of radicals where there is some angular dependence of the reaction channel, like the $H^\bullet + O_2$ reaction. Most $OH^\bullet$ radical reactions will fall into this category, and we might expect to find that the high-pressure limiting rate constant applies if solvation is not a large effect. The reduction of spin exchange rate between muonium and Ni_2^+ ions at high temperature may also be explained by the reduced caging effect, on the assumption that spin exchange is weak in this system. However, we disagree with

Percival in applying this collision frequency analysis to hydrated electron reactions. These are essentially a special type of electron-transfer reaction, and a modified version of the Marcus theory must apply. Therefore, several quantities such as the ΔG for the reaction and reorganization energy may account for a non-Arrhenius or decreased rate constant at elevated temperatures.

(51) Hack, W.; Preuss, A. W.; Wagner, H. G. *Ber. Bunsen-Ges. Phys. Chem. Chem. Phys.* **1979**, *83*, 212.
(52) Thrush, B. A.; Wilkinson, J. P. T. *Chem. Phys. Lett.* **1981**, *84*, 17.
(53) Sridharan, U. C.; Qiu, L. X.; Kaufman, F. *J. Phys. Chem.* **1982**, *86*, 4569.
(54) Keyser, L. F. *J. Phys. Chem.* **1986**, *90*, 2994.